ISIJ International, Vol. 50 (2010), No. 4, pp. 574–582

Characterization of the Bake-hardening Behavior of Transformation Induced Plasticity and Dual-phase Steels Using Advanced Analytical Techniques

Ilana B. TIMOKHINA,[1)] E. V. PERELOMA,[2)] S. P. RINGER,[3)] R. K. ZHENG[3)] and P. D. HODGSON[1)]

1) Centre for Material and Fibre Innovation, Deakin University, Geelong, Vic 3217 Australia.
2) School of Mechanical, Materials and Mechatronic Engineering, The University of Wollongong, Wollongong, NSW 2522 Australia. 3) Australia Key Centre for Microscopy and Microanalysis, University of Sydney, NSW 2006 Australia.

(*Received on April 6, 2009; accepted on February 6, 2010*)

The bake-hardening (BH) behavior of TRansformation Induced Plasticity (TRIP) and Dual-Phase (DP) steels after intercritical annealing (IA) has been studied using transmission electron microscopy, X-ray diffraction and three dimensional atom probe tomography. It was found for the DP steel that carbon can segregate to dislocations in the ferrite plastic deformation zones where there is a high dislocation density around the "as-quenched" martensite. The carbon pinning of these dislocations, in turn, increases the yield strength after aging. It was shown that bake-hardening also leads to rearrangement of carbon in the martensite leading to the formation of rod-like low temperature carbides in the DP steel. Segregation of carbon to microtwins in retained austenite of the TRIP steel was also evident. These factors, in combination with the dislocation rearrangement in ferrite through the formation of cells and microbands in the TRIP steel after pre-straining, lead to the different bake-hardening responses of the two steels.

KEY WORDS: transformation-induced plasticity; TRIP steel; DP steel; bake-hardening; Transmission Electron Microscopy; Atom Probe Tomography; dislocation structure.

1. Introduction

In recent years there has been an increasing demand for high strength, tough and ductile steels for the automotive and structural industries, as they provide an optimum combination of properties, cost and productivity. For automotive applications the main approach to achieving high strength with good formability has been through the development of multiphase steels, such as Dual Phase (DP) and Transformation Induced Plasticity (TRIP).[1,2)] DP steels are characterised by the presence of a soft ferrite matrix, which provides good formability, and hard martensite islands, that control the strength of the steel.[3)] The TRIP steel microstructure also contains a soft ferrite matrix, to control the formability, but with bainite and retained austenite to provide the strength and high levels of work hardening.[4,5)] In addition, the complex microstructure in both steels can increase the work-hardening rate in other ways, such as through the formation of mobile dislocations in the soft ferrite matrix and martensite twinning in the DP steel and the transformation of retained austenite to martensite during forming in the TRIP steel.[6–9)]

The bake-hardening (BH) treatment has been used for both TRIP and DP steels to increase the yield strength of steels in the final body structure for the same thickness of steel sheet. The bake hardening concept was initially developed for very soft low carbon steels to provide improved dent resistance. However, in these new advanced high strength steels BH has been reported to increase the yield strength by up to 100 MPa after 2 to 10% pre-straining (PS) using thermal conditions that simulate the paint baking of the car body.[10–12)]

Three different strengthening stages of BH in the multiphase steels have recently been identified[11)]: (i) Cottrell atmosphere formation around mobile dislocations in ferrite, (ii) the precipitation of low temperature carbides in ferrite and (iii) formation of clusters and particles in martensite/bainite.[11)] The previous research has also shown that the dislocation substructure formed in polygonal ferrite as a result of martensite transformation during processing of the DP steel, and the microstructural changes such as TRIP effect in the TRIP steels, during pre-straining affect the BH behavior.[12)] Hence, there are four major factors, that can affect the bake-hardening behavior: (i) the amount of carbon in solution, (ii) the formation of the dislocation substructure in ferrite, (iii) differences in the kinetics of strain ageing of the phases and (iv) the effect of strain partitioning between soft and hard phases during straining.[13,14)]

Although the importance of these aspects for the aging behavior of intercritically annealed multiphase steels has been highlighted by many authors[11–16)] using different techniques, limited data has been published on the carbon content of the various phases, solute cluster formation and segregation of carbon to dislocations during BH. High

© 2010 ISIJ

spatial resolution methods, such as Atom Probe Tomography (APT), can be used to accurately study these features. The main objective of the current study was to increase the fundamental understanding of the effect of carbon on the aging behavior of different phases in multiphase DP and TRIP steels using a unique combination of TEM and APT.

2. Experimental

Both steels with the compositions shown in **Table 1** were produced by a standard cold rolling and intercritical annealing (IA) at 780°C for 180 s after that the DP was quenched, while the TRIP steel was cooled to 400°C and held for 300 s followed by quenching.

Tensile samples were prepared from each material and pre-strained (PS) in tension to 5% and then baked at 175°C for 30 min. The BH conditions were chosen based on the maximum hardness response.

Room temperature mechanical properties of the samples after IA and after PS/BH were determined using an Instron 4500 servohydraulic tensile testing machine with a 100 kN load cell. The crosshead speed was fixed at 0.5 mm/min. Subsize samples with a 25 mm gage length, 6 mm in width and 2 mm in thickness were used to minimize the amount of material. A series of six experiments was used to define the average values of ultimate and yield strengths, total and uniform elongations. The yield strength was defined by the 0.2% offset method.

The bake-hardening response was measured as the difference between the upper yield strength after bake-hardening treatment and the flow stress after pre-straining.[17]

Optical microscopy and image analysis software (Adobe Photoshop™ equipped with image analysis plug-ins) were used to estimate the volume fraction of ferrite by area percent as the ratio of the total detected phase area to image frame. Eight to ten images were used to estimate the average value.

X-ray diffraction on a Philips PW 1130 (40 kV, 25 mA) diffractometer was used to identify the volume fraction of retained austenite and corresponding carbon content.[18] The retained austenite content was calculated from the integrated intensities of the $(200)_\alpha$, $(211)_\alpha$, $(200)_\gamma$ and $(220)_\gamma$ peaks using the direct comparison method.[18] (*PHILIPS is a trademark of Philips, Holland.)

The carbon concentration in the retained austenite lattice was calculated using the following equation[19]:

$$a_\gamma=(0.363067+0.0783/(1+0.2151(100/\text{wt\%C}-1)))\times(1+(24.92-1/(1+0.2151(100/\text{wt\%C}-1)))\times10^{-6}(T-727) \quad (1)$$

The microstructure was characterised using transmission electron microscopy (TEM), on a Philips CM 20, operated at 200 kV. Samples for TEM were polished by twin jet electropolishing using a solution of 5% perchloric acid in methanol at −20°C and an operating voltage of 30 V. (**PHILIPS, is a of Philips Electronic Instruments Corp., Mahwah, NJ.)

The dislocation density was calculated by using an equation[20]:

$$\Lambda=2N_L/Lt \quad (2)$$

Table 1. Compositions of studied steels.

Steel		C	Si	Mn	Al	Cu	Cr	Ti
TRIP	wt%	0.12	1.77	1.39	0.031	0.005	0.02	0.003
	at%	0.55	3.44	1.38	0.062	0.004	0.02	0.004
DP	wt%	0.036	1.065	1.08	0.018	0.004	0.083	-
	at%	0.17	2.09	1.08	0.037	0.0035	0.088	-

Table 2. Mechanical properties of steels.

Steel		UTS, (MPa)	YS, (MPa)	Total El, (%)	Uniform El, (%)	Average BH Response, (MPa)
TRIP	IA	795±10	520±10	31±2	27±3	60±3
	PS/BH	810±8	735±5	27±2	21±3	
DP	IA	633±10	425±10	24±3	23±2	80±2
	PS/BH	678±7	676±7	17±3	14±2	

where N_L is the number of intersections with dislocations made by random lines of length L, and t is the foil thickness. The foil thickness (t) was determined from intensity oscillations in the two-beam convergent beam electron diffraction (CBED) patterns.[21]

Selected samples were studied using carbon replicas prepared from 2% Nital etched samples that were carbon coated. The carbon films were then removed from the surface using 10% Nital and were collected on a Cu grid. The particle analysis of the replicas was performed using Qualitative energy dispersive X-ray spectroscopy (EDXS). The nominal beam diameter was ~2–3 nm and the diameter of condenser aperture was 50 μm.

Atom Probe Tomography (APT) analysis used the Local Electrode Atom Probe (LEAP) at the University of Sydney. The samples for APT were electropolished using standard two-stage procedure.[22] The local electron atom probe was operated at a pulse repetition rate of 200 kHz, a 0.2 pulse fraction and with a sample temperature of 80 K.

3. Results

3.1. Mechanical Properties of the DP and TRIP Steels after IA and PS/BH

Both steels demonstrated a good combination of mechanical properties and continuous yielding behavior after IA (**Table 2**, **Figs. 1**(a), (c)).

The strain-hardening rate curves for both steels showed a continuous exponential decrease (Figs. 1(b), (d)). The PS/BH post processing led to the appearance of upper and lower yield points and yield point elongation for both steels (Fig. 1(a), (c)). However, the stress–strain curve of the TRIP steel at the upper yield point showed a more rounded shape compared to the DP steel. The strain-hardening rate of the DP steel revealed the transition from a continuous yielding behavior to the formation of a local minimum followed by a higher strain-hardening rate (Fig. 1(b)), while the strain hardening rate of the TRIP steel still showed a continuous decrease (Fig. 1(d)). Both steels displayed a noticeable bake-hardening response, with increases in the yield and ultimate tensile strengths, while the elongation deteriorated in both steels (Table 2). The differences in the stress–strain and strain-hardening rate behaviors of TRIP and DP steels after IA and after PS/BH could be a result of microstructural features formed after PS/BH. The micro-

© 2010 ISIJ

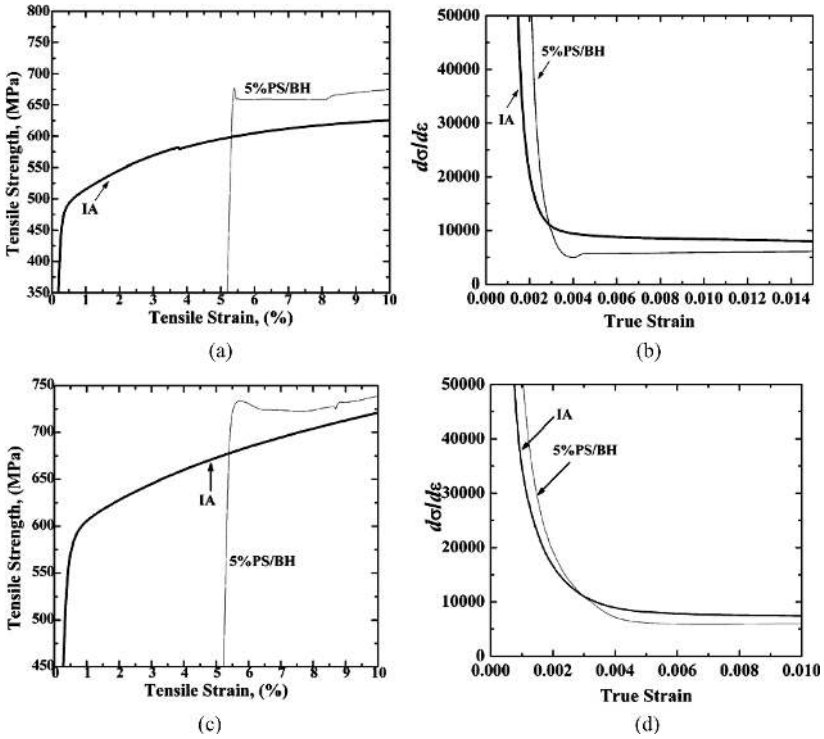

Fig. 1. Representative stress–strain and strain-hardening rate curves: (a, b) DP steel and (c, d) TRIP steel, after IA and PS/BH.

structural characterization of these features is the focus of the next section.

3.2. Microstructural Characterisation of DP Steel before and after PS/BH Using TEM and APT

Microstructural characterisation of the DP steel after IA revealed the presence of 75±5% polygonal ferrite, 15±4% martensite and a small amount of retained austenite and bainite (**Figs. 2**(a) and (b)). The ferrite grain size of the DP steel was 9.0±1.9 μm.

The study of dislocation substructure in ferrite is important here since the density of mobile dislocations and formation of dislocation substructure, such as cells or bands, can control the BH behavior. An average dislocation density of $0.96\pm0.04\times10^{14}\,m^{-2}$ for the polygonal ferrite grains was calculated based on the TEM study of the areas distant from any grain boundary or polygonal ferrite/martensite interface (**Table 3**). However, TEM observations of the areas in the vicinity of martensite islands displayed a local increase in the dislocation density to $5\pm0.8\times10^{14}\,m^{-2}$ (Table 3, Fig. 2(c)) near the ferrite/martensite interface.

This is likely to be due to the stress propagation of the martensite into the soft ferrite matrix associated with the volume increase when martensite forms. Some martensite/retained austenite constituents were observed between ferrite grains in the DP steel (Fig. 2(d)). A large number of fine and coarse Fe_3C carbides in the ferrite matrix of the DP steel was also observed (Fig. 2(e)).

Since the BH behaviour of the DP steel is controlled by the concentration of interstitial carbon in ferrite to pin the dislocations, it is important to measure the solute redistribution in the various phases. APT was used to study the partitioning of carbon and alloying elements in the phases of the DP and TRIP steels before and after PS/BH. APT also has the necessary spatial and mass resolution to perform analysis on solute atom segregation to dislocations, which is deemed to be the main mechanism involved in the bake-hardening of multiphase steels. The matrix composition was calculated from the volumes without visible elemental segregation or particle formation based on the number of atoms analyzed and using noise subtraction. The average carbon content of ferrite in the DP steel was found to be 0.06±0.01 at%, while for the martensite it was 2.8±0.2 at% (**Table 4**).

The carbon atom maps of ferrite and martensite showed the homogeneous redistribution of carbon within the volume. The Si content of ferrite was slightly higher than the average from the steel composition, while Mn was almost the same (Tables 1 and 4). The levels of Si and Mn were higher in martensite than in ferrite (Table 4). Since the retained austenite and bainite volume fraction in the DP steel was relatively low, these phases were not detected by APT in the samples examined.

The TEM microanalysis on the DP steel after PS/BH did not reveal significant microstructural changes except an increase in the average dislocation density of the ferrite (Table 3) and the evidence of martensite twinning (Fig. 2(f)).

The main aim of the APT study on the PS/BH DP steel was to find the carbon segregation to dislocations in ferrite since this mechanism is expected to control the BH behavior. This study is very challenging task, due to the small volume of analysis of the three-dimensional atom probe compared to the physical extent of the dislocations. However, several atom maps of the DP samples after PS/BH showed an increased level of solute carbon along linear features (**Fig.** 3(a)). For clarity, all other elements are not shown. These features are likely to be the dislocations dec-

© 2010 ISIJ

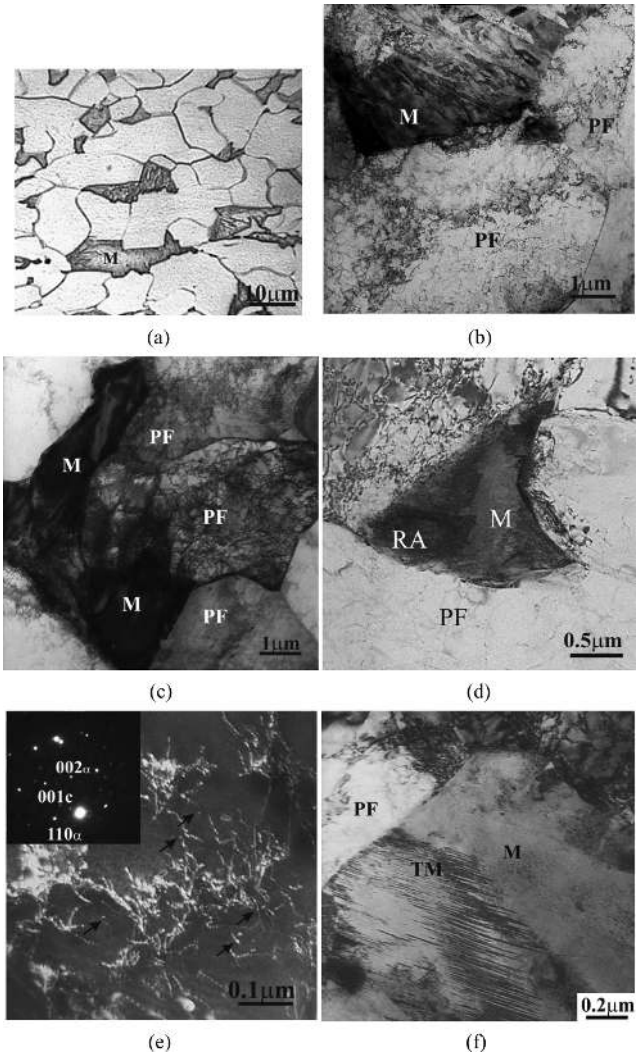

Fig. 2. Microstructure of DP steel: (a) optical micrograph, general view after IA, (b) TEM micrograph, general view after IA, (c) local increase in the dislocation density of ferrite near martensite after IA, (d) martensite/retained austenite constituent after IA, (e), dark field micrograph of Fe_3C carbides in ferrite of DP steel from $(001)_c$ ($[\bar{1}10]_\alpha//[\bar{1}00]_c$) after IA, and (f) twinned martensite after PS/BH. PF is polygonal ferrite, RA is retained austenite, M is martensite, TM is twinned martensite. Arrows indicate carbides.

Table 3. Dislocation density of polygonal ferrite. PF is polygonal ferrite and M is martensite.

	DP			TRIP	
	As-rec		PS/BH	As-rec	PS/BH
	average	PF/M interface	average	average	average
Dislocation Density, $x10^{14}m^{-2}$	0.96±0.04	5±0.8	2.4±0.09	1.75±0.09	2.7±0.05

Table 4. Phase compositions based on the concentration of major alloying elements (at%) determined using APT and calculated based on the number of atoms after IA. Iron is balance.

Steel	Phase		Element, (at%)		
			C	Si	Mn
DP	Ferrite		0.06±0.01	2.3±0.2	0.97±0.05
	Martensite		2.8±0.2	3.4±0.02	1±0.08
TRIP	Ferrite		0.02±0.01	3.9±0.03	0.9±0.03
	Austenite		4.6±0.02	3.9±0.05	1.02±0.03
	Bainite	Bainitic Ferrite	0.2±0.03	2.8±0.02	1.5±0.02
		Austenite	5.1±0.2	4.4±0.05	1.2±0.03

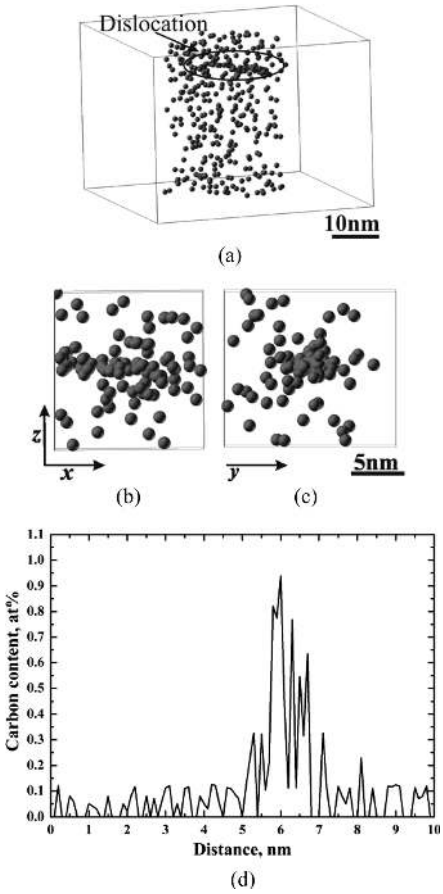

Fig. 3. Representative carbon atom map (a), selected carbon atom maps in two perpendicular directions (b, c) of carbon segregation to dislocation and corresponding carbon concentration profile across the dislocation observed in the polygonal ferrite of DP steel after PS/BH treatment.

Table 5. Phase compositions based on the concentration of major alloying elements (at%) determined using APT and calculated based on the number of atoms after PS/BH. Iron is balance.

Steel	Phase	Element, (at%)		
		C	Si	Mn
DP	Ferrite	0.04±0.005	2.5±0.1	1±0.1
	Martensite	2.2±0.1	2.7±0.1	1.1±0.08
TRIP	Ferrite	0.02±0.01	3.8±0.07	1±0.05
	Austenite	4.2±0.1	3.9±0.02	1.1±0.06

orated by carbon, as the rod-like shape of an atmosphere is clearly visible in the carbon atom map taken from the perpendicular direction (Fig. 3(b)).

A radius of gyration of the Cottrell atmosphere around the dislocation was calculated based on the maximum separation method and found to be $l_g(y)=1$ nm and $l_g(x)=2.8$ nm. The segregation of carbon to dislocations occurred more likely in ferrite area in vicinity of martensite island, where the dislocation density is higher. The average carbon content of ferrite after PS/BH was also calculated from the analysed volumes without any visible segregation. It was found to be 0.04 ± 0.005 at% (**Table 5**), which is lower than average ferrite carbon content after IA.

While all atom maps of martensite crystals in the DP steel after IA had a uniform redistribution of carbon, APT study of PS/BH samples revealed the formation of rod-like fine iron carbides in individual martensite islands and also

© 2010 ISIJ

in martensite regions of martensite/retained austenite constituents. The representative carbon atom map and iso-concentration surface of martensite/retained austenite constituent after PS/BH treatment are shown in **Figs. 4**(a) and (b). It could be seen clearly that one part of this sample has homogeneous redistribution of carbon without visible segregation of carbon atoms, while another part has non-homogeneous redistribution of carbon (Figs. 4(a) and (b)).

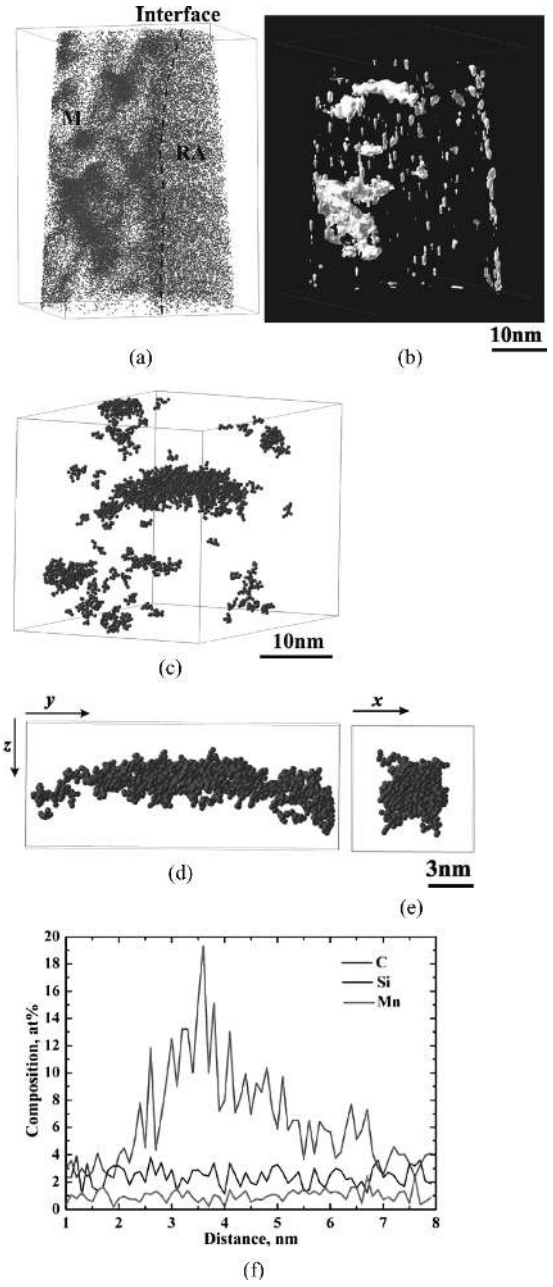

Fig. 4. Carbon atom maps (a, c–e) and 8 at% carbon iso-concentration surface (b) of martensite/retained austenite constituent after PS/BH in DP steel, dashed lines in (a) show suggested interface line between decomposed martensite and austenite, selected carbon atom map, which represents the area of interest (c), selected carbon maps of rod-like carbide (selected box in (a)) in two perpendicular directions (d, e) and corresponding carbon concentration profile across carbide (f). RA is retained austenite and M is martensite. The matrix atoms for (c)–(e) were suppressed with the maximum separation methods with $d_{max}=0.7$ nm. The total number of atoms analyzed in (a) is 3463215.

The average carbon content of sample volume with homogeneous redistribution of carbon was 5.0±0.5 at% and is close to the carbon value in retained austenite. The average carbon content of the matrix from the part of the sample with non-homogeneous redistribution of carbon was 2.2±0.1 at% (Table 5), which is twice less than the carbon content in austenite and corresponds to the concentration of C in martensite. The average carbon content and Si content of martensite after PS/BH were lower than after IA. This data correlates well with TEM results showing the formation of some martensite/retained austenite islands in the DP steel after IA and PS/BH.

The precipitates formed in martensite volume of the sample, had clearly defined crystallographic structure of atoms *i.e.* clearly visible planes (Figs. 4(c)–(e)). These rod-like carbides were aligned in three different directions and had an average radius of 3±0.5 nm. A representative compositional profile across a carbide is shown in Fig. 4(f). The carbon content of carbides varied from 10 at% to 20 at% C, while the levels of Si and Mn were similar to the matrix composition (Fig. 4(f)). These compositions are close to the composition of low temperature $Fe_{32}C_4$ or $Fe_4C_{0.63}$ carbides. Moreover, the maximum separation method revealed the formation of small carbon clusters in martensite (Fig. 4(c)). The term "cluster" was used for the local segregation of ~20 to 100 carbon atoms, where there is no clearly defined crystallographic structure observed within the cluster.

3.3. Microstructural Characterisation of TRIP Steels before and after PS/BH Treatment Using TEM and APT

The TRIP steel contained ~70±3% polygonal ferrite, ~20±3% retained austenite and a small volume of martensite and bainite (**Figs. 5**(a) and (b)). The ferrite grain size was 4±1.5 μm, which is less than half that of the DP steel. The *average* dislocation density in the ferrite was almost

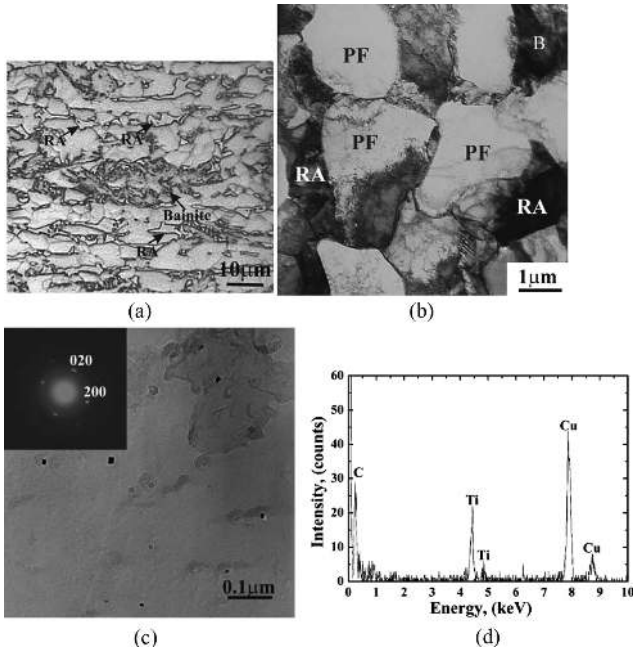

Fig. 5. Optical (a) and TEM (b) micrographs of TRIP steel after IA, carbon replica (a) and corresponding EDX spectrum (Cu peak is from Cu grid) from TiC carbides in the TRIP steel (zone axis for diffraction pattern (insert) is $[001]_c$).

© 2010 ISIJ

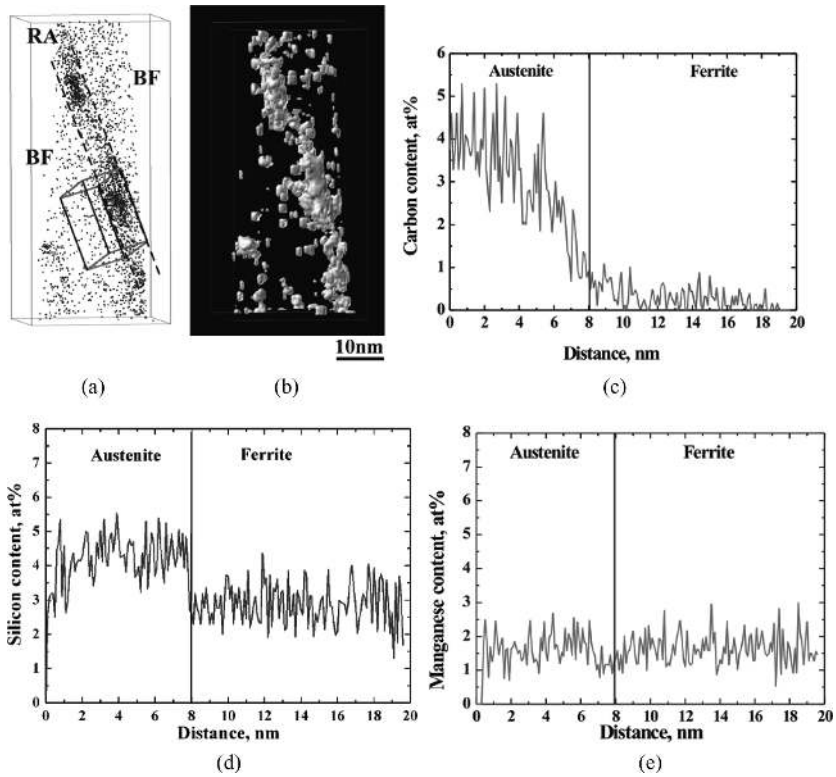

Fig. 6. Bainite in the TRIP steel after IA: (a) carbon atom map, dashed lines indicate retained austenite/bainite interface, (b) 1.75 at% C iso-concentration surface, (c–e) concentration profile along y direction of selected box shown in (a). RA is retained austenite and BF is bainitic ferrite.

twice higher than in the DP steel (Table 3). The average carbon content of the retained austenite calculated by X-ray was 5.00 ± 0.02 at%. The analysis of particles showed the formation of TiC with a cubic lattice structure and a lattice parameter of $a = 0.424$ nm (Figs. 5(c) and (d)).

The average carbon content of ferrite in the TRIP steel after IA calculated using APT was 0.02 ± 0.001 at%. This value was significantly lower than in the ferrite of the DP steel. The Si content of ferrite in the TRIP steel was also higher than the average from the steel composition, while the Mn content was lower (Table 4). Compositional analysis of several atom maps confirmed the presence of retained austenite in the TRIP steel (Table 4). Based on the carbon content and the size of retained austenite islands, two types of retained austenite were identified: (i) coarse and (ii) retained austenite in bainite. APT of coarse retained austenite revealed a uniform redistribution of carbon within the volumes with an average carbon content of 4.6 ± 0.02 at%, which is close to the value calculated by X-ray. This retained austenite is proposed to have formed between polygonal ferrite grains. Several atom maps showed the areas, which can be described as a mixture of carbon-enriched (5.1 ± 0.2 at%) and carbon-depleted (0.2 ± 0.03 at%) regions (**Figs. 6**(a) and (b), Table 4).

It appears that the carbon-depleted region in this island represents bainitic ferrite, while the carbon-enriched region is retained austenite located between the bainitic ferrite laths. A very important observation is that bainitic ferrite was characterised by a significantly higher carbon content (~ 0.2 at%), lower Si content (~ 2.8 at%) and higher Mn (~ 1.5 at%) level than the polygonal ferrite (Table 4). The compositional profile across the retained austenite/bainitic ferrite interface showed that there was no segregation of C, Mn and Si to the interface (Figs. 6(c)–(e)). The absence of partitioning of the substitutional elements between the retained austenite and bainitic ferrite is consistent with other work[23] related to a diffusionless type of austenite to bainite transformation. Moreover, the absence of carbon segregation indicates that the interface is semi-coherent, with a high degree of coherency.[24] The retained austenite in bainite had a plate-like shape with an average thickness of 16 ± 2 nm (Figs. 6(a), (b)) and slightly higher carbon content than the coarse blocks of the RA, which would be due to further carbon enrichment during the bainite transformation.

The PS/BH of the TRIP steel led to a decrease in the volume fraction of retained austenite to 12 ± 1% and an increase in the average dislocation density of polygonal ferrite (Table 3). The most affected grains were in the vicinity of martensite crystals (**Fig. 7**(a)). Since the volume fraction of martensite after IA of the TRIP steel was low, it is likely that these martensite crystals are formed during PS by strain-induced transformation. The formation of dislocation cells in the polygonal ferrite grains in the vicinity of martensite islands was also observed in the TRIP steel (Fig. 7(b)). Some of the martensite crystals contained twins as did some of the retained austenite crystals (Figs. 7(a), (c)). PS/BH led to the formation of iron carbides between the bainitic ferrite laths in the TRIP steel (Fig. 7(d)).

As mentioned above, the study of solute segregation during BH using APT is experimentally difficult to perform and in some cases, unsuccessful. Nonetheless, several carbon atom maps of the TRIP steel after PS/BH from different directions showed the segregation of carbon to par-

© 2010 ISIJ

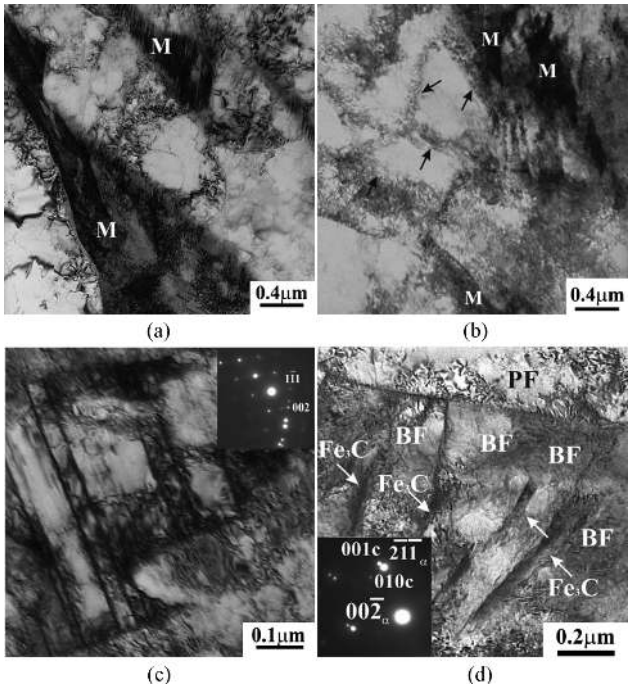

Fig. 7. TEM micrographs of TRIP steel after PS/BH: (a) dislocation tangles in ferrite between strain-induced twinned martensite islands, (b) dislocation cell substructure in ferrite (arrows indicate cell walls), (c) twinned austenite (zone axis is $[110]_\gamma$, twin plane is $(\bar{1}11)_\gamma$), (d) bright TEM image of carbide formation between the bainitic ferrite laths ($[112]_\alpha$//$[100]_c$) (arrows indicate carbides between bainitic ferrite). PF is polygonal ferrite, M is martensite.

ticular atomic planes within the sample volumes (**Figs. 8**(a)–(f)). These planes cross the samples at different angles (Figs. 8(a), (b)).

The compositional analysis of the matrix revealed that this segregation was in the retained austenite, which contains average carbon content of 4.2 ± 0.1 at% (Table 5). The concentration profiles across these planes showed carbon enrichment to 6.5 ± 0.5 at%, while the Si and Mn concentrations were similar to those in the matrix (Fig. 8(g)). The average thickness of these planes was 1 ± 0.2 nm. As mentioned above, TEM proved the formation of austenite twins during PS as a result of plastic relaxation (Fig. 7(c)). Moreover, the previous TEM study[12] of the bake-hardening behaviour of the TRIP steel has also shown the formation of two set of deformation microtwins with preferential zone axis of $\langle 110\rangle_\gamma$ and twin plane of $\{111\}_\gamma$ or zone axis of $\langle 112\rangle_\gamma$ and $\{111\}_\gamma$ twin plane within some of retained austenite islands. Based on the TEM and APT data, it was speculated that the segregation of carbon occurred during BH to the *twin planes* formed in retained austenite as a result of PS. It worth emphasizing that it is extremely difficult to obtain the crystallographic information from APT data. Although in selected cases, it is possible to determine the distance between the planes in the matrix, in our case γ-Fe, and find their orientation, which allows to define the twin plane orientation. **Figure 9**(a) shows the Fe map and determined distance between the Fe atomic planes to be 0.2 nm. It appeared to be the d-spacing between $\{111\}_\gamma$ planes. Since one of twin plane with carbon segregation is parallel to $\{111\}_\gamma$ (Fig. 9(b)), it makes possible to determine the crystallographic orientation of this twin plane, which is also $\{111\}_\gamma$. The angle between the twin planes with carbon segregation was measured using several atom maps and was $\sim35\pm4°$. Taking into account the experimental error, it could be suggested that these twin planes represented $(111)_\gamma$ and $(1\bar{1}1)_\gamma$ intersecting at 39.5°. The formation of similar twinning substructure containing two sets of deformation twins on two intersecting $\{111\}_\gamma$ planes has been reported[25,26] for TWIP steels.

Compositional analysis of ferrite in the TRIP steel after PS/BH did not find any changes in the levels of elements (Tables 4 and 5).

4. Discussion

As mentioned above, the classical explanation of the BH behaviour in steels is based on unlocking of mobile dislocations in ferrite by a high stress during straining or, in the case of very strong pinning, by creating new dislocations at the points of stress concentration. For the DP steel, the main factor that might affect BH is the formation of mobile dislocations in ferrite near by martensite/ferrite interface as a result of the volume expansion accompanying the austenite to martensite transformation during quenching. APT after PS/BH showed segregation of carbon to linear features, which are believed to be as dislocations, in ferrite of DP steel. Hence, the presence of the upper yield point on the stress–strain curve of DP steel after PS/BH and an increase in yield strength could be a result of unlocking of the mobile dislocations in ferrite, that were pinned by carbon atmospheres around dislocations. APT also confirmed the formation of rod-like carbides in martensite after the PS/BH with a composition close to the composition of low temperature $Fe_{32}C_4$ or $Fe_4C_{0.63}$. The conventional ε carbides (~30 at% C) were not observed by APT. This correlates well with the results published by Abe on formation of carbides in martensite during BH.[27] The explanation for carbide formation could be that the PS leads to a rapid stress-induced ordering of solute carbon atoms into preferred positions according to the stress fields of the dislocations.[27] Then the stress-induced migration of carbon atoms towards the dislocation could occur at the BH temperature with additional carbon atoms migrating to the dislocations to form fine particles. The dislocations in martensite provide suitable sites for the formation of carbides at 175°C. One further point that should be noted is that 30 min is sufficient time for carbon to move to the dislocations in martensite and form carbides. The formation of low temperature carbides during decomposition of martensite as a continuos process has been also observed in thermomechanically processed TRIP steel after PS/BH.[28] It starts from the formation of carbon clusters as precursors to carbide formation and ends with the formation of equilibrium Fe_3C carbide. The formation of these carbides would contribute to the increase in tensile strength after PS/BH. As mentioned above, TEM and APT confirmed the presence of retained austenite/martensite constituent in the microstructure of the DP steel and decomposition of martensite component during BH, while the retained austenite remained stable. It could be speculated that carbon from martensite could diffuse to austenite during BH, since the solubility of carbon

© 2010 ISIJ

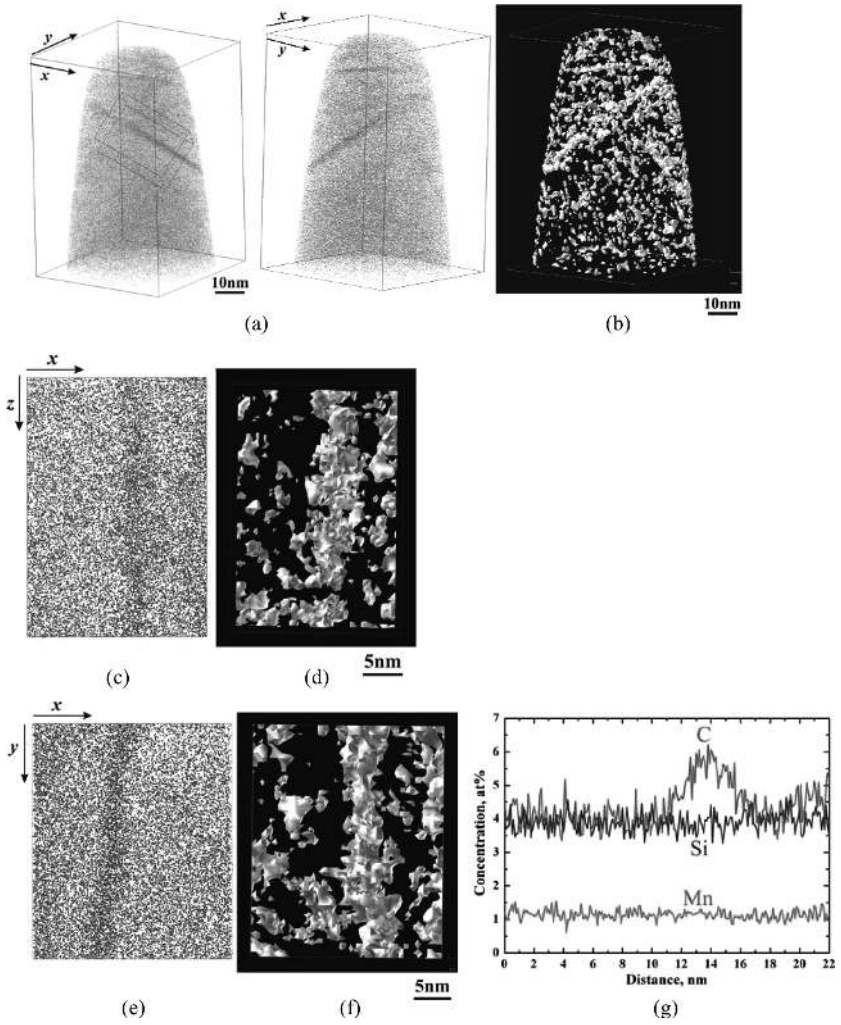

Fig. 8. Representative carbon atom maps from two different directions (a) and 7.5 at% C iso-concentration surface (b) showing the carbon segregation to the atomic plane in retained austenite island in the TRIP steel after PS/BH treatment, selected carbon atom maps shown in (a) in two perpendicular directions (c and e) and corresponding 7.5 at% C iso-concentration surfaces (d and f), and compositional profile across retained austenite island (g).

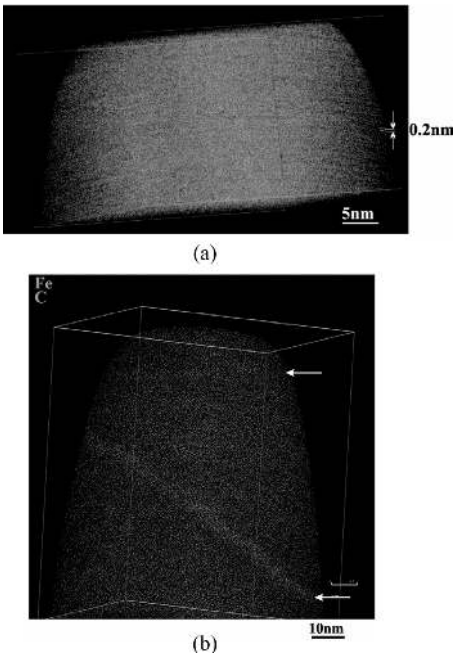

Fig. 9. Fe atom map showing interplanar distance (a) and Fe–C atom map showing segregation of C at microtwin boundaries (b). Arrows in (b) indicate segregation at microtwin planes.

is much greater in austenite than in ferrite (martensite). This would lead to an increase in the chemical stability of the retained austenite during BH treatment and its stability towards strain-induced transformation.

The importance of the APT study for the TRIP steel after IA is that the information on phase compositions of all phases could be obtained. The average carbon level of retained austenite calculated by XRD and APT showed quite similar results; 5 at% and 4.85 at% respectively. The carbon content of retained austenite calculated using Thermo-Calc® software[29] at 400°C (T_0) was 4 at%, which is lower than those measured by XRD and APT. This could be explained by partitioning of carbon to retained austenite during the bainite transformation.

It appeared that the BH behaviour in TRIP steel is mainly defined by the formation of the dislocation cell structure in ferrite and high carbon content of ferrite (Table 4). This could be presumably associated with an additional effect of retained austenite to martensite transformation and austenite twinning during PS that increases the number of mobile dislocations in ferrite. The stress–strain behaviour of the TRIP steel after the PS/BH treatment showed that a larger strain was required to achieve the work-hardening region of the stress–strain curve. The assumption implies that it is un-

© 2010 ISIJ

likely that the yield point in the TRIP steel after PS/BH occurred due to the locking and unlocking the dislocations by high stress. Alternatively, the flow stress was reduced due to generation of new mobile dislocations in the ferrite.

One important point worth mentioning is that APT verified the segregation of carbon to particular planes in the austenite after PS/BH. The segregation of carbon to the defects such as dislocations or twins in the retained austenite has been recently observed in the martensitic and bainitic steels.[23)]

5. Conclusions

The study of the bake-hardening mechanism in the multiphase TRIP and DP steels using advanced microscopic techniques has proved that the more pronounced bake-hardening response in the DP steel could be associated with carbon segregation to dislocation in ferrite. The bake-hardening treatment leads to formation of low temperature carbides and carbon clusters in martensite of the DP steel and the segregation of carbon to the microtwins in the retained austenite of the TRIP steel, which could, in general affect the strength–ductility balance of both steels.

Acknowledgements

The authors would like to acknowledge the support of the Ford Motor Company and Australia Research Council (ARC) Linkage Scheme. One of the authors (PDH) also acknowledges the support of the ARC Federation Fellowship scheme. The authors also would like to acknowledge the assistance in tensile testing from Mr. B. Clarke.

REFERENCES

1) Y. Sakuma, O. Matsumura and H. Takechi: *Metall. Trans. A*, **22A** (1991), 489.
2) R. G. Davies: *Metall. Trans. A*, **9** (1978), 41.
3) A. H. Nakagawa and G. Thomas: *Metall. Trans. A*, **16** (1985), 831.
4) O. Matsumura, Y. Sakuma and H. Takechi: *Trans. Iron Steel Inst. Jpn.*, **27** (1987), 570.
5) K. Sugimoto, N. Usui, K. Kobayashi and S. Hashimoto: *ISIJ Int.*, **32** (1992), 1311.
6) O. Matsumura, Y. Sakuma and H. Takechi: *Scr. Metall.*, **21** (1987), 1301.
7) G. R. Speich and V. A. Demarest: *Metall. Trans. A*, **12A** (1981), 1419.
8) V. F. Zackay, E. R. Parker, D. Fahr and R. Bush: *Trans. ASM*, **60** (1967), 252.
9) M. Kinoshita and A. Nishimoto: *CAMP-ISIJ*, **3** (1990), 1780.
10) B. C. De Cooman: *Current Opinion in Solid State and Mat. Science*, **8** (2004), 285.
11) T. Waterschoot, A. K. De, S. Vandeputte and B. C. De Cooman: *Metall. Trans. A*, **34** (2003), 781.
12) I. B. Timokhina, P. D. Hodgson and E. V. Pereloma: *Metall. Trans. A*, **38** (2007), 2442.
13) K. Sugimoto, M. Kobayashi, H. Matsushima and S. Hashimoto*: Trans. Jpn. Soc. Mech. Eng.*, **16A** (1995), 80.
14) K. Sugimoto, M. Kobayashi, S. Yasuki and S. Hashimoto: *Mater. Trans., JIM*, **36** (1995), 632.
15) L. J. Baker, S. R. Daniel and J. D. Parker: *Mater Sci. Technol*, **18** (2002), 355.
16) T. Senuma: *ISIJ Int.*, **41** (2001), 520.
17) A. K. De, S. Vandeputte and B. C. De Cooman: *Scr. Mater.*, **44** (2001), 695.
18) B. D. Cullity: Elements of X-Ray Diffraction, Addison-Wesley Publishing, London, England, (1978), 411.
19) M. Onink, C. M. Brakman, F. D. Tichelaar, E. J. Mittemeijer, S. van der Zwaag, J. H. Root and N. B. Konyer: *Scr. Metall. Mater.*, **29** (1993), 1011.
20) P. B. Hirsch, R. B. Nicholson, A. Howie, D. W. Pashley and M. J. Whelan: Electron Microscopy of Thin Crystals, Butterworths, London, (1965), 51.
21) P. M. Kelly, A. Jostsons, R. G. Blake and J. G. Napier: *Phys. Stattus Sollidi*, **31** (1975), 771.
22) M. K. Miller: Atom Probe Tomography, Kluwer, Academic/Plenum Publisher, New York, (2000), 28.
23) F. G. Caballero, M. K. Miller, S. S. Babu and C. Garcia-Mateo: *Acta Mater.*, **57** (2007), 381.
24) H. K. D. H. Bhadeshia and D. V. Edmonds: *Acta Mater.*, **28** (1980), 1265.
25) G. Frommeyer, U. Brux and P. Neumann: *ISIJ Int.*, **43** (2003), No. 3, 438.
26) D. Barbier, N. Gey, S. Allain, N. Bozzolo and M. Humbert: *Mater. Sci. Eng.*, **500** (2009), 196.
27) H. Abe: *Scand. J. Metall.*, **13** (1984), 226.
28) E. V. Pereloma, M. K. Miller and I. B. Timokhina: *Metall. Trans. A*, **39** (2008), 3210.
29) J. O. Anderson, T. Helinder, I. Hogland and B. Sundman: *Calphad*, **26** (2002), 273.

© 2010 ISIJ